

Cross-linked conjugated polymers based on triazine and poly-branched polycyclic thiophene for improved photocatalytic hydrogen evolution

Zibin Li^a, Ya Chu^b, Fanpeng Meng^a, YunYun Dong^a, Jinsheng Zhao^{a,*}, Huayang Zhang^{c,*}, Xiujuan Zhong^{a,*}

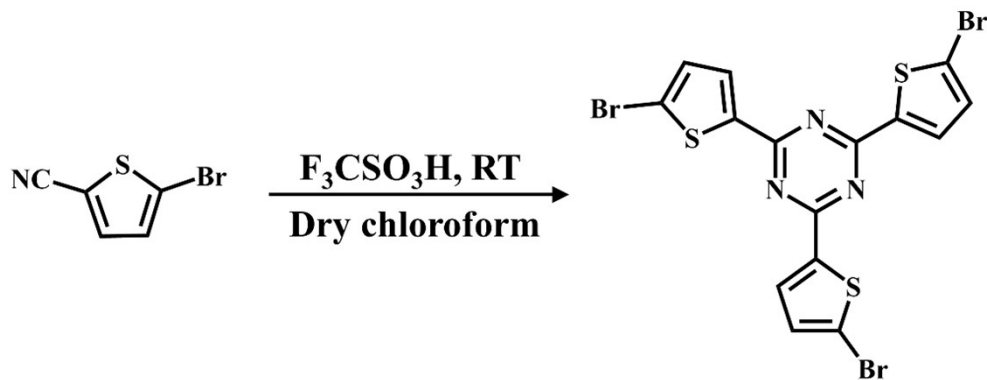
^aShandong Key laboratory of Chemical Energy Storage and Novel Cell Technology, College of Chemistry and Chemical Engineering, Liaocheng University, Liaocheng, 252059, P.R. China.

^bSchool of Physics Science and Information Technology, Liaocheng University, Liaocheng, 252059, P.R. China

^cSchool of Chemical Engineering, The University of Adelaide, North Terrace, Adelaide, SA 5005, Australia

Corresponding authors: E-mail Address: j.s.zhao@163.com (J.S. Zhao); huayang.zhang@adelaide.edu.au; (H.Z. Zhang); zhongxiujuan@lcu.edu.cn (X.J. Zhong)

1. Synthesis of 2,4,6-tris(5-bromothiophene-2-yl)-1,3,5-triazine (M1) ¹



4.0 g (21.3 mmol) of 5-bromothiophene-2-carbonitrile was dissolved in 500 mL of dry chloroform, and 12.8 g (85.2 mmol) of trifluoromethanesulfonic acid was dropped into the solution at 0 °C. The resultant solution was magnetically stirred for 2 hours at 0 °C, and then the temperature of the solution was risen to room temperature for 48 hours. The mixture was rinsed with distilled water, and dried by anhydrous magnesium sulphate. The solution was obtained by filtration. Then, the solvent was distilled off by vacuum distillation. Finally, the crude product was purified by recrystallization in toluene to obtain a white needle solid. ¹H NMR (500 MHz, CDCl₃), δ 7.97 (d, *J* = 4.0 Hz, 3H), 7.17 (d, *J* =

4.0 Hz, 3H) (Fig. S1).

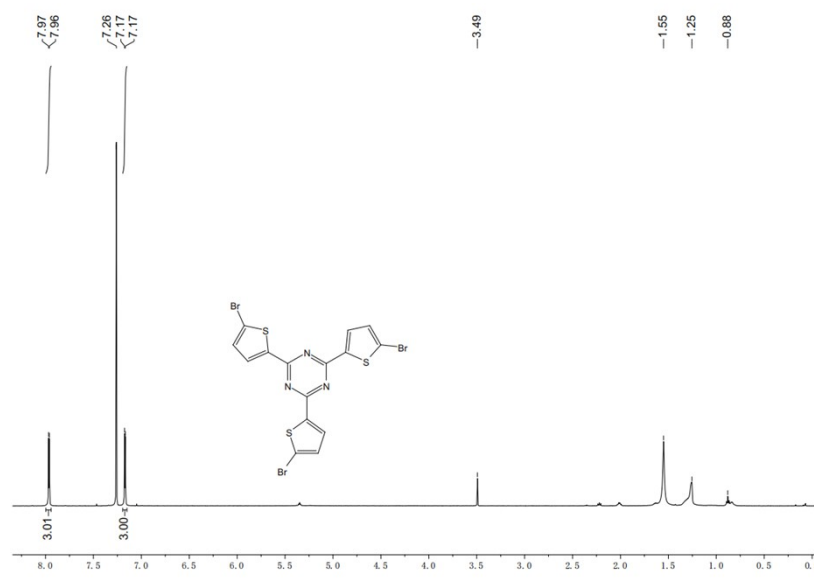


Fig. S1. ^1H NMR spectrum of M1

2. Characterization methods

Fourier transform infrared (FT-IR) spectra was carried out on a Nicolet Avatar 360 FT-IR spectrometer with KBr pellets. Solid state magic angle spinning ^{13}C CP-MAS NMR measurement was measured on a Bruker Avance III HD 600 MHz wide Bore Solid NMR spectrometer at a MAS rate of 10 kHz. Powder X-ray diffraction (PXRD) was carried out with 2θ ranging from 5 to 80° using a Rigaku D/max 2500 X-ray advanced diffractometer with Cu-K α radiation, and a step scan mode was adopted with a scanning step of 0.02° . X-ray photoelectron spectroscopy (XPS) was performed with an ESCALAB 250Xi spectrometer to get the sample's surface chemical states. The thermogravimetric analysis (TGA) of the photocatalysts was conducted on a Netzsch STA449C TG/DSC thermal analyzer under a nitrogen atmosphere between 20°C and 800°C . The morphology of the materials was measured by scanning electron microscope (SEM) (Thermo Fisher Scientific FIB-SEM GX4). The distribution and composition of the elements of the photocatalysts were also roughly evaluated by Scanning electron microscopy-energy dispersive X-ray spectrometry (SEM-EDS). The transmission electron microscopy (TEM) was examined to investigate the structural characterization using JEM-2100F. Surface areas and pore size distributions were measured by Nitrogen isotherm adsorption-desorption at 77.3 K using ASAP 2460-3

(Micromeritics) volumetric adsorption analyzer. The UV-vis diffuse reflectance spectroscopy (UV-vis DRS) of polymers was measured by an Agilent Carry 5000 spectrophotometer (CA, USA). Photoluminescence (PL) spectra were collected on an F-7000 FL spectrophotometer. Time-resolved PL spectra were measured using a time-correlated single-photon counting system (FLS1000). The Electron paramagnetic resonance spectroscopy was measured using a China instru & Quantumtech (Hefei) EPR200-Plus with continuous-wave X band frequency.

3. Calculation method

The frontier molecular orbitals (FMOs), electrostatic potential surface (ESP) and Mulliken charge distribution of PhDBD-CPP and ThDBD-CPP molecular are calculated on B3LYP/6-31G (d, p) basis set using Gaussian 16 software package. The calculations of charge density differences of H chemisorbed, electron localization function (ELF) and hydrogen evolution reaction Gibbs energies are performed under the framework of density functional theory (DFT) with the Vienna Ab-initio Simulation Package (VASP).² The spin polarization projection augmented wave (PAW) method³ and the Perdew-Burke-Ernzerhof (PBE) electron exchange-correlation function of generalized gradient approximation (GGA) are used to describe the interactions between valence electrons and ionic core for all atoms. All geometries are optimized with an energy cut-off (500 eV) until the convergence criteria for energy and force are less than 1×10^{-5} eV and 0.01 eV/Å, respectively.

The definition of H atom adsorption Gibbs free energy (ΔG_{H^*}) as the following equation:

$$\Delta G_{H^*} = \Delta E_H + \Delta E_{ZPE} - T\Delta S_H$$

Where ΔE_H is H atom adsorption energy and was calculated by equation:

$$\Delta E_H = E_{(catalyst+H)} - E_{(catalyst)} - E_{H_2} / 2$$

Here $E_{(catalyst+H)}$, $E_{(catalyst)}$ are the energies of PhDBD-CPP and ThDBD-CPP with and without H atom adsorption, respectively. E_{H_2} is one hydrogen gas energy.

Additionally, ΔE_{ZPE} stands for zero points energy and was calculated from the vibration frequency. ΔS_H represents the entropy difference between the atomic hydrogen

adsorbed and the gas phases and can approximately be regarded as $1/2(S_{H_2})$ (S_{H_2} is the entropy of gas phase H_2 at standard conditions).

4. Electrochemical measurements

Electrochemical impedance spectra (EIS) and Mott-Schottky plot were measured on a CHI660E (Chenhua, Shanghai) electrochemical workstation in a standard three-electrode system. The sample-modified Pt-disk electrode with a diameter of 3 mm was used as the working electrode, and Pt flake and Ag/AgCl as the counter and reference electrodes, respectively. The mixture slurry was made as follows: polymer photocatalysts (10 mg), isopropyl alcohol (1 mL), and 30 μ L of Nafion (0.921 g/mL), which was dispersed by ultrasound in a water bath for 30 min. The mixture slurry (10 μ L) was dropped on the platinum plate electrode and dried under an infrared lamp before the measurements, which was used as the working electrode. EIS experiments were performed in a frequency range from 1 Hz to 100 kHz at 0.2 V, and Na_2SO_4 aqueous solution (0.5 M, pH=6.8) was used as the electrolyte.

5. Transient photocurrent measurements

The transient photocurrent responses (I-t) were also measured on CHI660E (Chenhua, Shanghai) electrochemical workstation in a standard three-electrode system, including a Pt sheet as the counter electrode (1 cm \times 1 cm), an Ag/AgCl electrode as the reference electrode, and a catalyst-modified indium tin oxide (ITO) electrode as the working electrode. The applied voltage difference on the working electrode is 1 V vs. Ag/AgCl. 0.5 M Na_2SO_4 aqueous solution was used as an electrolyte. The catalyst slurry was prepared by adding 10 mg of catalyst to a mixture solution of 1 mL isopropyl alcohol and 30 μ L Nafion (5%), and the slurry was fully dispersed in an ultrasonic cleaner for 30 min before use. For the preparation of the ITO electrode, 20 μ L of the above polymer slurry was coated on the ITO/glass electrode with a surface area of 1 cm \times 1 cm and dried under an infrared lamp.

6. Transient absorption measurements

The femtosecond transient absorption spectra were recorded on Newport's Femtosecond Stimulated Raman Spectrometer (United States). The femtosecond laser (Newport, United States) has a wavelength of 800 nm at 1kHz, and the full width at

half-maximum is 100 fs. The 800 nm pulse is divided into two pulses by a beam splitter at a 9:1 ratio. A femtosecond pulse passes through a BBO to generate a frequency doubling pulse as a pump pulse. As a probe pulse, the other pulse passes through the delay line so that the pump and probe light arrive at the sample with a time difference. The probe pulse is concentrated on optically nonlinear transparent media (CaF₂). The probe pulse and the pump pulse remain coincident in time and space. Transient absorption kinetics traces were fitted using software from CarpetView. The transient absorption experiments were conducted at room temperature.

7. AQY measurements

The apparent quantum yield (AQY) of the photocatalysts was measured with a monochromatic light obtained by using bandpass filters of 380, 420, 475, 550, and 600 nm with energy intensities of 33.7, 37.2, 55.7, 50.4, and 40.2 mW cm⁻², respectively.

The AQY at a given wavelength was calculated by the following equation:⁴

$$AQY = 2 \frac{N_0}{N_p} \times 100\% = \frac{2 \times M \times N_A \times h \times c}{S \times P \times t \times \lambda} \times 100\%$$

Where M is the amount of H₂ (mol) produced, N_A is Avogadro constant (6.02×10^{23} mol⁻¹), h is the Planck constant (6.626×10^{-34} J · s), c is the speed of light in vacuum (3×10^8 m/s), S is the irradiation area (19.6 cm² in our experiment), P is the intensity of irradiation light (W/cm²), t is the irradiation time (s), λ is the wavelength of the monochromatic light (m).

8. Photocatalytic hydrogen evolution experiment

All the photocatalytic experiments were carried out in an all-glass automatic online trace gas analysis system (CEL-PAEM-D8, Beijing China Education Au-Light Technology Co., LTD.). First of all, 10 mg of ball-milled polymer, 10.56 g of AA, 10 mL of NMP, and 46 mL of distilled water were added to a 100-mL Pyrex glass reaction vessel, and then 4 mL of NaOH solution (5 M) was added to adjust the pH of the mixed solution to 4. Afterwards, the mixture is sonicated for 10 min to obtain a uniformly dispersed suspension, and then 4 μL of chloroplatinic acid (1 wt%) as cocatalyst was added into the solution. The system was degassed for half an hour to remove the dissolved oxygen, the suspension was irradiated with a 300 W Xe lamp and stirred (with

or without a UV cut-off filter ($\lambda > 420$ nm)). The reaction unit is kept at a temperature of 10 °C with a circulating water cooling system. The hydrogen evolution was analyzed by gas chromatography (CEAULIFGT, GC-7920) equipped with a TCD detector every 0.5 h. The analysis utilized a TDX-01 column, with argon as the carrier gas, and the column oven temperature was set to 80 °C.

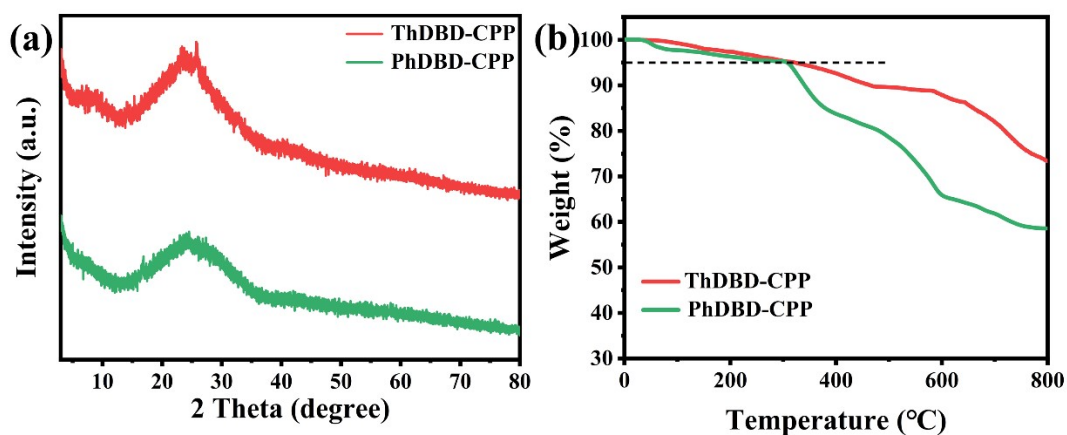


Fig. S2. (a) PXRD patterns of the polymers. (b) TGA curves of the polymers.

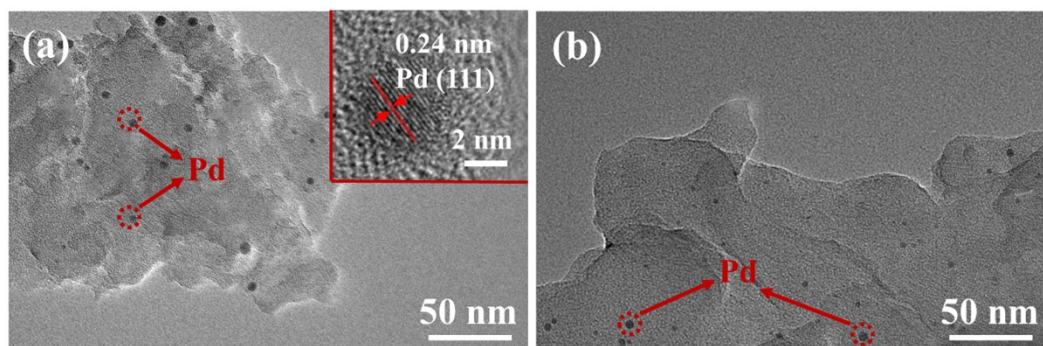


Fig. S3. TEM images of ThDBD-CPP (a) and PhDBD-CPP (b).

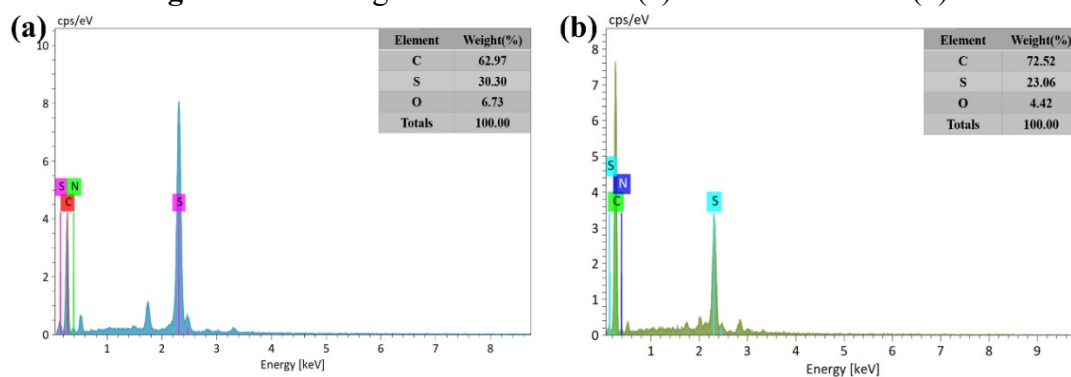


Fig. S4. EDX images of ThDBD-CPP (a) and PhDBD-CPP (b).

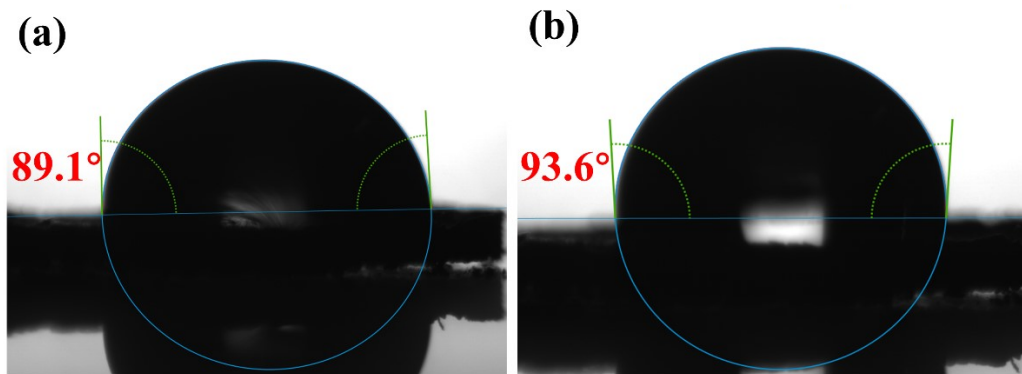


Fig. S5. Water contact angles of ThDBD-CPP (a) and PhDBD-CPP (b).

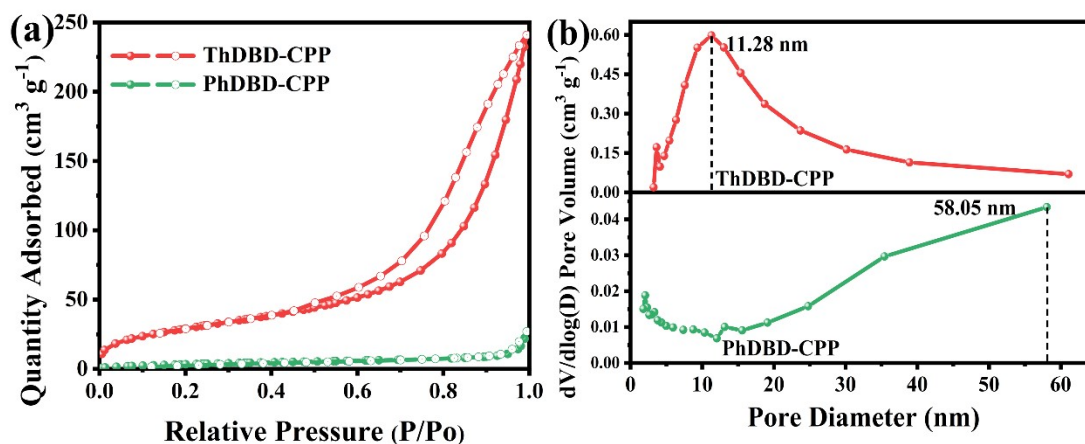


Fig. S6. N_2 adsorption-desorption isotherms (a) and pore size distribution (b) of the polymers.

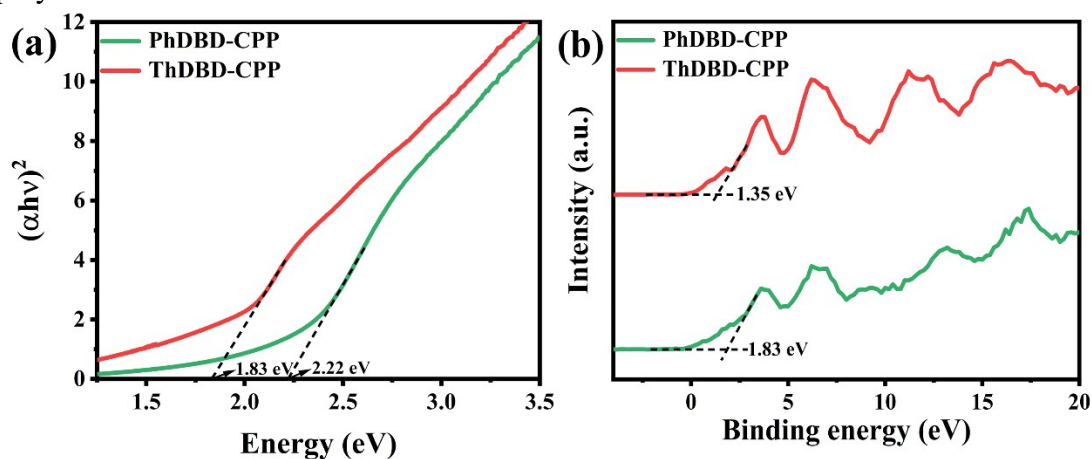


Fig. S7. Tauc plot (a) and VB-XPS spectra (b) of the polymers.

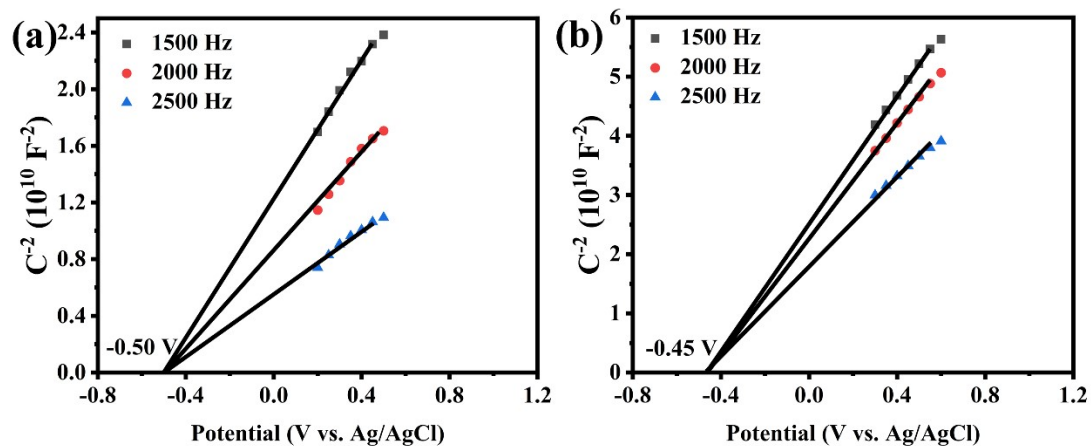


Fig. S8. Mott-Schottky plots of ThDBD-CPP (a) and PhDBD-CPP (b) at different frequencies in an aqueous solution of Na_2SO_4 (0.5 M).

Table S1. Photocatalytic hydrogen evolution performance of the reported CPP photocatalysts.

Photocatalyst	Cocatalyst	Sacrificial agent	HER ($\text{mmol g}^{-1} \text{h}^{-1}$)	AQY (%)	Refs
PCP4e	No	TEA	9.43 (full-arc light)	0.34 (350 nm)	5
PCP10	No	TEA	8.63 (full-arc light)	1.05 (400 nm)	6
TBT-BDT	3 wt% Pt	TEOA	4.2 ($\lambda > 400$ nm)	—	7
TzSPy	3 wt% Pt	TEOA	10.3 (AM1.5G)	—	8
Py-TPA-CMP	3 wt% Pt	AA	19.2 ($\lambda > 420$ nm)	15.3 (420 nm)	9
$\text{C}_3\text{N}_3\text{-SO}$	3 wt% Pt	TEOA	2.97 ($\lambda > 420$ nm)	0.58 (420 nm)	10
Triazine-Ph-CPP	No	TEOA	3.50 ($\lambda > 420$ nm)	61.50 (365 nm)	11
CTF-BT/Th	3 wt% Pt	TEOA	6.60 ($\lambda > 420$ nm)	7.30 (420 nm)	12
ThDBD-CPP	1 wt% Pt	AA	30.36 (full-arc light)	8.8 (475 nm)	This work

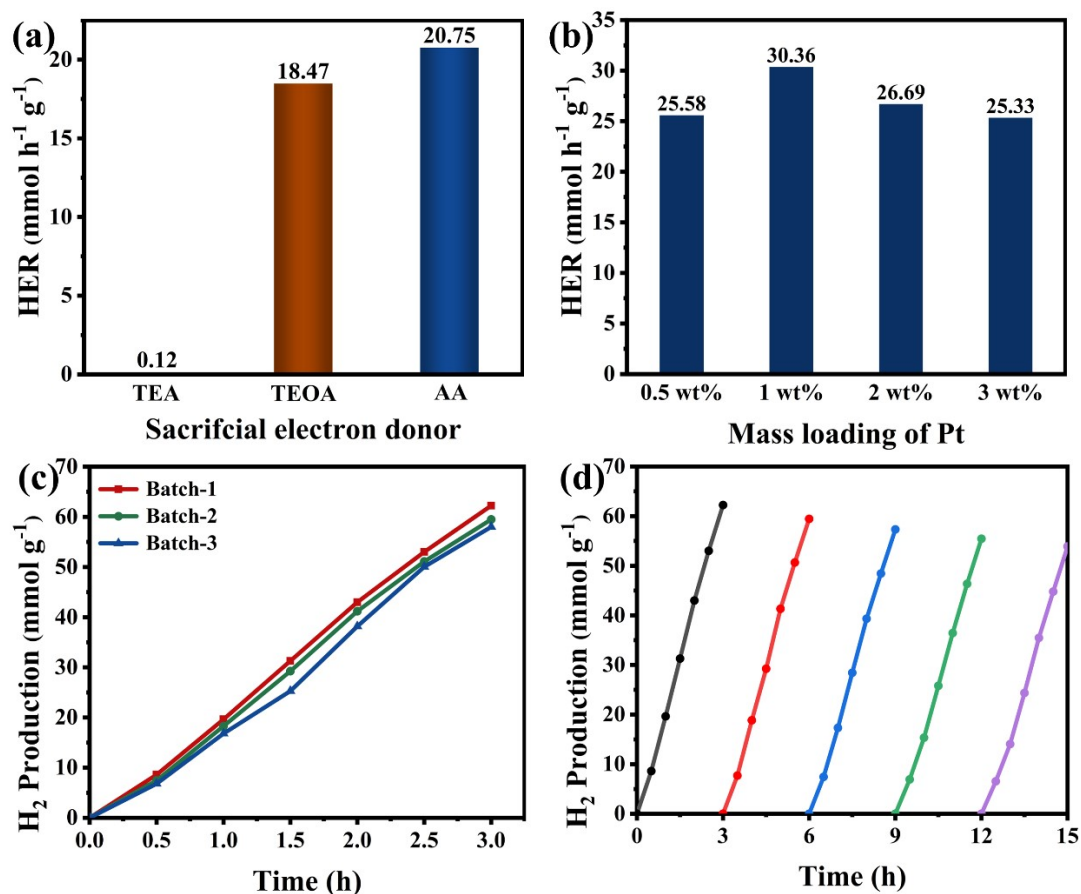


Fig. S9. HERs of ThDBD-CPP with different sacrificial agents (a), different Pt contents (b), different batches (c) and continuous test (d) under full arc light ($\lambda > 300 \text{ nm}$).

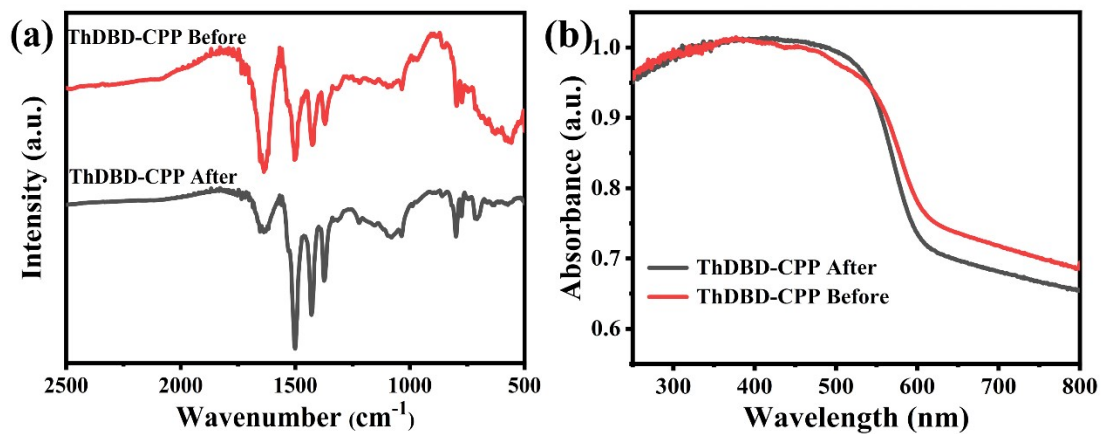


Fig. S10. FT-IR spectra (a) and UV-vis DRS (b) of ThDBD-CPP before and after irradiation under full-spectrum irradiation.

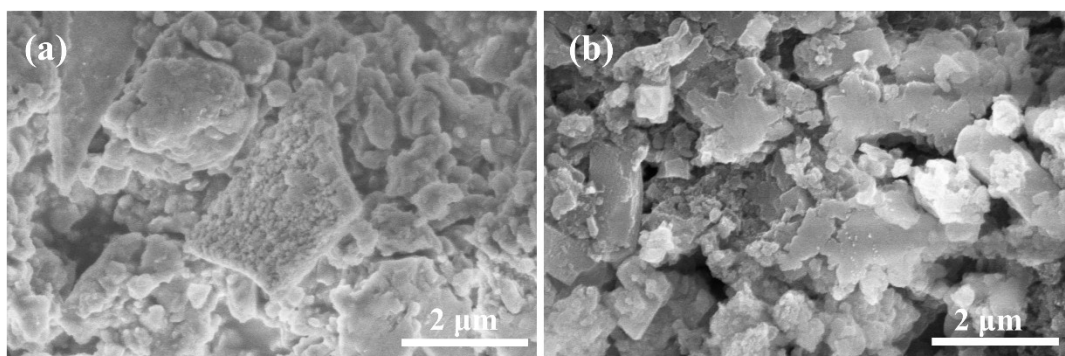


Fig. S11. SEM images of ThDBD-CPP before (a) and after (b) irradiation under full-spectrum irradiation.

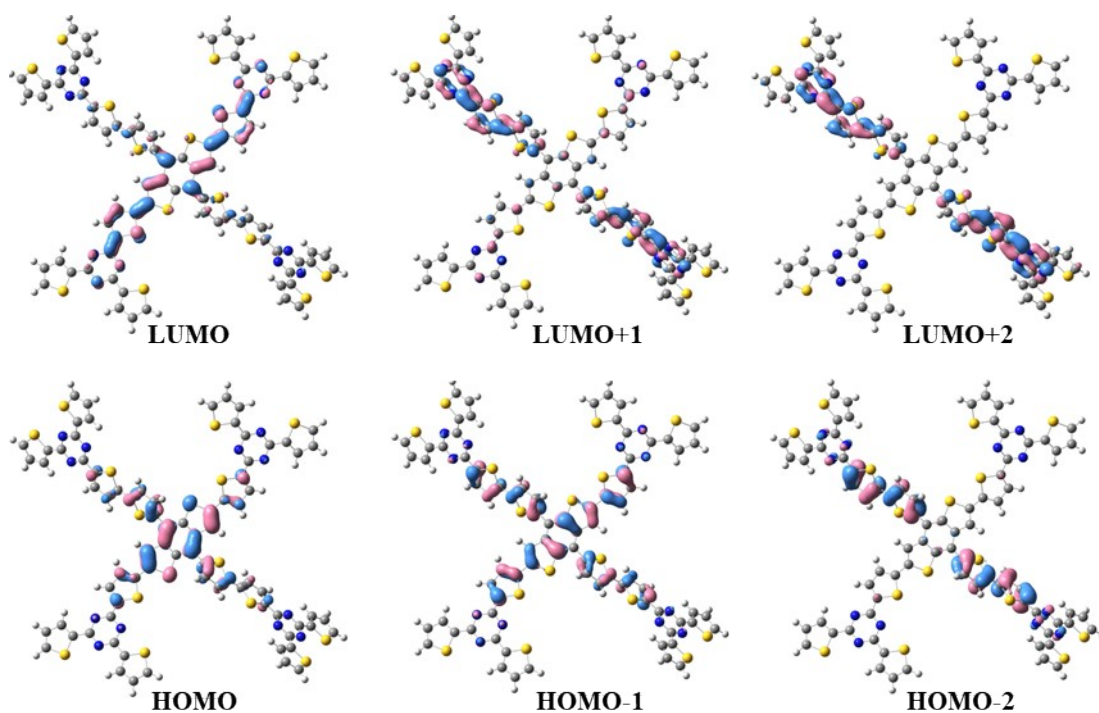


Fig. S12. Electron orbital distributions of the molecular orbitals of ThDBD-CPP.

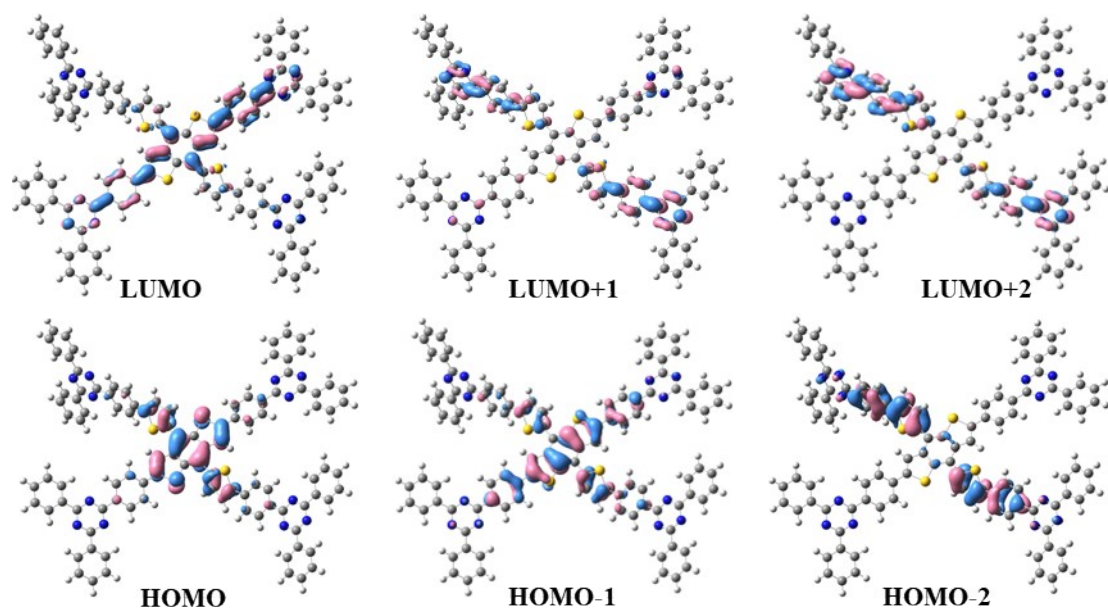


Fig. S13. Electron orbital distributions of the molecular orbitals of PhDBD-CPP.

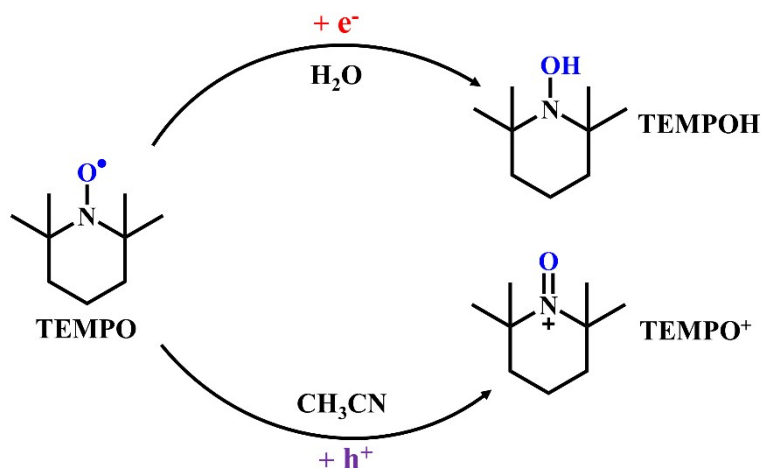


Fig. S14. Trapping mechanism of TEMPO.

References

- (1) S. L. Zhang, F. Zhao, G. Yasin, Y. Y. Dong, J. S. Zhao, Y. Guo, P. Tsiakaras and J. Zhao, *J. Colloid Interface Sci.*, 2023, **637**, 41-54.
- (2) G. Kresse and J. Furthmüller, *Phys. Rev. B*, 1996, **54**, 11169-11186.
- (3) G. Kresse and D. Joubert, *Phys. Rev. B*, 1999, **59**, 1758-1775.
- (4) X. Han, F. Zhao, Q. Q. Shang, J. S. Zhao, X. J. Zhong and J. H. Zhang, *ChemSusChem*, 2022, **15**, e202200828.
- (5) L. W. Li, Z. X. Cai, Q. H. Wu, W. Y. Lo, N. Zhang, L. X. Chen and L. P. Yu, *J. Am. Chem. Soc.*, 2016, **138**, 7681-7686.
- (6) L. W. Li, W. Y. Lo, Z. X. Cai, N. Zhang and L. P. Yu, *Macromolecules*, 2016, **49**, 6903-6909.
- (7) F. L. Yi, Q. Yang, X. Y. Li, Y. Q. Yuan, H. M. Cao, K. W. Liu and H. J. Yan, *J. Solid State Chem*, 2023, **318**, 123769.
- (8) J. Yang, M. M. Zhai, J. J. Qin, Y. H. A. Liu, W. B. Hu, H. Yang and K. Wen, *Polym. Chem.*, 2022, **13**, 5769-5774.

- (9) M. G. Mohamed, M. H. Elsayed, A. M. Elewa, A. F. M. EL-Mahdy, C. H. Yang, A. A. K. Mohammed, H. H. Chou and S. W. Kuo, *Catal. Sci. Technol.*, 2021, **11**, 2229-2241.
- (10) C. L. Ru, T. Zhou, J. Zhang, X. Wu, P. Y. Sun, P. Y. Chen, L. Zhou, H. Zhao, J. C. Wu and X. B. Pan, *Macromolecules*, 2021, **54**, 8839-8848.
- (11) J. L. Wang, G. C. Ouyang, Y. Wang, X. L. Qiao, W. S. Li and H. X. Li, *ChemComm*, 2020, **56**, 1601-1604.
- (12) W. Huang, Q. He, Y. P. Hu and Y. G. Li, *Angew. Chem. Int. Ed.*, 2019, **131**, 8768-8772.